Pathways of atomistic processes on TiN(001) and (111) surfaces during film growth: an *ab initio* study

D. Gall, S. Kodambaka, M. A. Wall, I. Petrov, and J. E. Greene[a)]
Department of Materials Science and the Frederick Seitz Materials Research Laboratory, University of Illinois, 104 South Goodwin, Urbana, Illinois 61801

(Received 2 January 2003; accepted 21 February 2003)

Density functional methods were used to calculate binding and diffusion energies of adatoms, molecules, and small clusters on TiN(001) and TiN(111) surfaces in order to isolate the key atomistic processes which determine texture evolution during growth of polycrystalline TiN layers. The surface energy for nonpolar TiN(001), 81 meV/Å^2, was found to be lower than that of both N- and Ti-terminated TiN(111) polar surfaces, 85 and 346 meV/Å^2. While N_2 molecules are only weakly physisorbed, Ti adatoms form strong bonds with both TiN(001), 3.30 eV, and TiN(111), 10.09 eV. Ti adatom diffusion is fast on (001), but slow on (111) surfaces, with calculated energy barriers of 0.35 and 1.74 eV, respectively. The overall results show that growth of 111-oriented grains is favored under conditions typical for reactive sputter deposition. However, the presence of excess atomic N (due, for example, to collisionally induced dissociation of energetic N_2^+ ions) leads to a reduced Ti diffusion length, an enhanced surface island nucleation rate, and a lower chemical potential on the (001) surface. The combination of these effects results in preferential growth of 001 grains. Thus our results provide an atomistic explanation for the previously reported transition from 111 to 001 texture observed for sputter deposition of TiN in Ar/N_2 mixtures with increasing N_2 partial pressure P_{N_2} and at constant P_{N_2} with increasing N_2^+/Ti flux ratios incident at the growing film. © *2003 American Institute of Physics.* [DOI: 10.1063/1.1567797]

I. INTRODUCTION

$B1$-NaCl structure titanium nitride (TiN) layers, deposited by reactive magnetron sputtering, are widely used as hard wear resistant coatings on cutting tools, as diffusion barriers in microelectronic devices, and as corrosion and abrasion resistant layers on optical components. In each of these applications, control of layer microstructure is crucial and determines the usefulness, performance, and lifetime of the coatings. Thus, there is a large literature on the relationship among deposition parameters, microstructure, and performance for a given application. However, little is known regarding the detailed atomistic mechanisms and reaction paths involved in TiN layer growth.

Experimental results show that polycrystalline TiN layers, typically sputter deposited from a Ti-metal target in pure N_2 or Ar/N_2 gas mixtures, have a columnar microstructure and exhibit competitive texture evolution.[1–5] During the initial stages of growth, primarily 001- and 111-oriented grains nucleate with approximately equal number densities.[1,2] However, grain growth rates are a function of crystalline orientation. This leads, with increasing film thickness, to the development of strong preferred layer orientation which is either 001 or 111, depending upon film deposition conditions.[1–5] The resulting film texture has, in turn, a determining effect on the overall coating performance due to highly anisotropic elastic properties and differences in grain sizes and layer density.[3,6] It is therefore of interest to understand the underlying physical processes that favor the growth of 001 and 111 oriented grains.

Competitive columnar grain growth has been modeled for fcc-metals using atomistic Monte Carlo simulations.[7] Layer texture and microstructure were found to be determined by the interplay of both thermodynamic and kinetic driving forces, with the most important parameters being surface energies and adatom mobilities, both of which are a strong function of crystal orientation. The primary experimental parameters determining the evolution of texture are the film growth temperature,[8] strain,[5,8] and, in the case of transition-metal nitrides, low-energy N_2^+-ion irradiation.[1,2,9,10]

Several models have been proposed to explain texture evolution in cubic transition-metal nitrides. Pelleg *et al.*,[11] and later Oh and Je,[4,5] proposed that the orientation of polycrystalline TiN films should initially be 001, corresponding to the lowest energy surface,[12] then evolve toward 111 with increasing thickness as the film develops compressive stress due to ion irradiation typically present during sputter deposition. The 111 texture becomes favored since the elastic modulus is lower in the [111] direction. The change in orientation in this model is driven by the film/substrate system minimizing the total free energy.

However, Greene *et al.*[1,2] later showed that varying the flux of incident low-energy (20 eV) N_2^+ ions during reactive TiN deposition has a dramatic effect on texture, without introducing strain, and attributed this to kinetic rather than thermodynamic effects. Growth at low temperatures and ion-fluxes resulted in 111-textured TiN layers while increasing

[a)]Electronic mail: greene@mrlxp2.uiuc.edu

 © 2003 American Institute of Physics

Downloaded 26 May 2003 to 128.113.37.128. Redistribution subject to AIP license or copyright, see http://ojps.aip.org/japo/japcr.jsp

the ion-to-metal flux ratio J_i/J_{Ti} to >5 led to fully 001-oriented films. The formation of 111 texture under low-flux conditions was ascribed to limited adatom mobilities on 111 surfaces, leading to larger cation residence times, and consequently, higher cation incorporation probabilities on 111 versus 001 oriented grains. In contrast, high-flux ion irradiation gives rise to increased surface diffusivity due to ion-adatom momentum transfer and therefore has an effect similar to raising the growth temperature. Thus, under high ion-flux conditions, texture evolves towards the lowest surface energy, which is the 001.[12]

These models provide some insight into the general relationships between experimental parameters and layer microstructures while highlighting the effects of strain, ion irradiation, and anisotropies in surface energies, adatom mobilities, and elastic constants. However, they do not provide a detailed understanding of the atomistic processes controlling TiN texture evolution. In this article, we present the results of *ab initio* density functional calculations carried out in an attempt to examine the role of processes—including the adsorption and desorption of Ti and N atoms and N_2 molecules, the diffusion of adatoms and admolecules, and atomic binding energies in clusters—on (001) and (111) surfaces which determine film texture evolution.

We find that 111-oriented grain growth is preferred under deposition conditions in which the incident particles are only Ti atoms and N_2 molecules. However, if the deposition flux contains a high density of atomic N, or collisionally dissociating N_2^+ ions, the corresponding increase in the steady state N coverage dramatically alters growth kinetics in favor of 001 texture. The presence of atomic N on the surface reduces the Ti adatom diffusion length, lowers the effective nucleation length of surface islands, and decreases the chemical potential on (001) surfaces. These effects lead to a reversal in the net intergrain cation deposition flux, which now proceeds from 111 to 001-oriented grains. Thus 001-texture evolution is favored under growth conditions with high N_2^+ ion-to-Ti fluxes J_i/J_{Ti}.

II. COMPUTATIONAL METHOD

All density functional calculations were performed using the Vienna *ab initio* simulation package (VASP)[13] which employs pseudopotentials, a plane-wave basis set, and periodic boundary conditions to determine the Kohn–Sham ground state. The generalized gradient approximation (GGA) of Perdew and Wang[14] was chosen to obtain the exchange-correlation functional. Ultrasoft Vanderbilt-type pseudopotentials[15] with core radii of 2.70 and 1.65 a.u. for Ti and N, respectively, provide reasonable total energy convergence with energy cutoffs E_{cut} of only 262 to 350 eV for the plane-wave basis set expansion.

Ti $2p$ electrons, which occupy states ≃30 eV below the Fermi level, were explicitly treated, i.e., they were considered as valence electrons and not included in the pseudopotential. This was necessary because calculating Ti adsorption energies on TiN(001) surfaces with pseudopotentials which contain Ti $2p$ electrons in the core results in diverging structural energy minimization and errors exceeding 1 eV.

The equilibrium lattice constant a_0 of TiN was obtained by fitting calculated total energies versus volume to the Murnaghan equation of state.[16] The computed result, 4.26 Å, is close to the experimental value of 4.24 Å and within the range of previously computed values, 4.23–4.26 Å, from density functional calculations employing various gradient corrected exchange correlation functionals.[17,18] The lattice parameter was maintained constant at the theoretical value for all computational results presented here.

The equilibrium gas-phase N_2 bond length of 1.11 Å, calculated using a $15\times15\times15$ Å^3 unit cell, is in excellent agreement with the experimental value of 1.10 Å.[19] We obtain a N_2 dissociation energy of 10.28 eV, within 3.5% of the experimental value, 9.93 eV.[20] The cohesive energy of TiN was found to be 14.33 eV per unit formula. This value includes corrections for the spin energies of Ti and N atoms, 2.24 and 3.11 eV, respectively. The experimental value for the formation energy for bulk TiN from N_2 gas and Ti metal is 3.5 eV per formula unit (Ref. 21) in good agreement with our calculated value of 3.70 eV, obtained by subtracting the sum of the computed cohesive energy for Ti, 7.73 eV per atom, and half the N_2 dissociation energy, from the calculated TiN cohesive energy.

Binding energies of adatoms in various configurations on TiN(001) and TiN(111) surfaces were obtained by subtracting the total energy of a clean surface from that containing adatoms. Using identical supercell sizes, plane-wave cutoff values, and *k* points for both calculations results in relatively rapid convergence of energy differences with respect to the above parameters. Test calculations were performed to check the convergence. Typical supercells for calculations on TiN(001) surfaces contain 108 atoms in three layers and a vacuum of 8.5 Å, corresponding to four interatomic spacings. Equilibrium configurations were obtained by relaxing the ionic positions of adatoms and first layer surface atoms using a conjugate-gradient algorithm. Subsurface atoms were fixed at their bulk positions. Calculations with larger supercells show that the uncertainty in binding energies due to limited lateral size (36 atoms per layer) is ≃0.08 eV, that due to vertical size (three layers) is ≃0.02 eV, and that due to relaxing only the top monolayer is ≃0.01 eV.

The TiN(111) surface is polar, i.e., alternating layers along the ⟨111⟩ direction contain exclusively N or Ti atoms. Consequently, the surfaces, which are either N- or Ti-terminated, exhibit charging. Test calculations were carried out to determine the minimum number of layers necessary to render the effect of back-surface charging negligible. Adatom binding energies calculated using supercells containing six and seven layers, corresponding to configurations with Ti- and N-terminated back surfaces, respectively, were equal to within ≃0.05 eV, showing that our typical (111) supercell containing seven layers with a total of 63 atoms provides reasonably accurate results. For calculations on the 111 surface, all atoms in the upper bilayer (one N and one Ti layer) were relaxed.

k-space sampling was performed according to the method of Monkhorst and Pack.[22] A grid of $2\times2\times1$ *k* points, where $\times1$ is in the direction perpendicular to the surface, was found sufficient for convergence of the total

Downloaded 26 May 2003 to 128.113.37.128. Redistribution subject to AIP license or copyright, see http://ojps.aip.org/japo/japcr.jsp

TABLE I. Calculated TiN surface energies. The polar (111) surfaces are in equilibrium with N_2 gas at 0 K.

Surface energies	Bulk terminated (meV/Å^2)	Relaxed (meV/Å^2)
TiN(001)	100	81
N-terminated TiN(111)	262	85
Ti-terminated TiN(111)	359	346

energy of typical supercells to within ≃0.07 eV. Surface energies were calculated with higher accuracy, using a grid of $15\times15\times1$ k points which yielded a convergence of <0.001 eV.

The overall computational accuracy of all energies presented in the following results section is, if not otherwise specified, 0.1 eV. This includes uncertainties due to the energy cutoff for plane-wave expansion, k-space sampling, pseudopotentials, unit cell size, number of atomic layers, and number of vacuum layers. Uncertainties introduced due to the generalized gradient approximation cannot easily be quantified, but should be ⩽0.1 eV. An exception might be calculated energy differences between N_2 molecules in the gas phase and N atoms in the solid or on the surface, since molecular dissociation energies are typically only good to within ≃0.3 eV using the GGA.[20] This is not of concern here, because our primary interest is in relative energy differences among surface adatom configurations.

III. RESULTS

A. Surface energies

The TiN(001) surface energy was determined using supercells containing up to eight atomic planes and six vacuum layers, corresponding to 16 atoms in an approximately $3\times3\times30$ Å^3 supercell. This yields values which are converged to <1 meV/Å^2. The calculated energy difference between the supercell and bulk TiN is 1.81 eV, corresponding to a bulk terminated (unrelaxed) TiN(001) surface energy of 100 ± 1 meV/Å^2 (see Table I). Allowing all atoms in the supercell to relax reduces the value to 81 ± 1 meV/Å^2, in agreement with the previously reported 81 meV/Å^2 (Ref. 18). A difference of only ≃20% between bulk-terminated and relaxed surface energies indicates a relatively weak surface relaxation. Positions of the Ti and N surface atoms in the relaxed surface are −0.12 Å and +0.06 Å from their corresponding bulk positions; surface Ti atoms move slightly into the layer while the N atoms protrude out of the surface. All atoms in the underlying layers are displaced less than the estimated accuracy of these calculations, 0.02 Å, from their bulk positions.

The surface energy of TiN(111) is not an intrinsically defined quantity, since the surface is polar and can therefore be either Ti- or N-terminated. Thus, we calculated energies for both cases and then subtracted [for Ti-terminated TiN(111)] or added (N-terminated) the chemical potential μ_N of N, to account for the extra Ti or N atom in the supercell. TiN growth is typically carried out in a N_2 overpressure which is several orders of magnitude higher than the equilibrium N_2 vapor pressure over TiN at the film growth tempera-

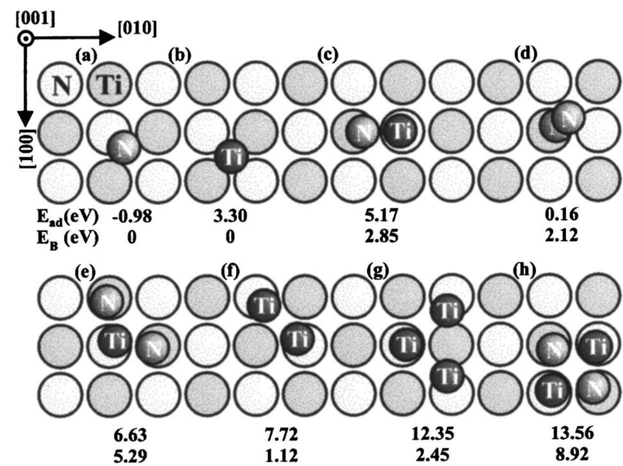

FIG. 1. Ti and N adatom configurations on TiN(001) with corresponding adsorption E_{ad} and binding E_B energies.

ture. Thus, it is a reasonable approximation to assume that the TiN surfaces are in equilibrium with gas phase N_2. We therefore simply set μ_N equal to 5.14 eV, half the calculated cohesive energy of the N_2 molecule, neglecting entropy terms and kinetic effects.

TiN(111) surface energies were calculated using supercells containing up to 13 layers, or 6.5 TiN bilayers. The N-terminated surface with atoms at bulk positions has an energy of 262 ± 1 meV/Å^2, which decreases to 85 ±1 meV/Å^2 when atoms are allowed to relax. This is a large energy gain, 177 meV/Å^2, and suggests considerable surface atom translation. The N-surface layer moves 0.23 Å inwards while second-layer Ti atoms relax outward by 0.22 Å. Thus the interlayer spacing of the upper bilayer decreases by 0.45 Å, 37% of the bulk spacing, 1.23 Å. Third and fourth layers exhibit much smaller displacements of −0.09 and <0.01 Å, respectively. We attribute the strong surface relaxation of N-terminated TiN(111) primarily to the surface dipole moment, caused by charge transfer from second-layer Ti to N surface atoms. The dipole moment, and consequently the total energy, is reduced as the interlayer spacing between N and Ti decreases.

Ti-terminated TiN(111) surfaces have considerably larger energies, 359 ± 1 meV/Å^2 for unrelaxed and 346 ±1 meV/Å^2 for relaxed structures. The surface relaxation is small compared to N-terminated TiN(111) since electrons from surface Ti atoms screen the surface dipole moment. The small energy gain of 13 meV/Å^2 upon relaxation is reflected in small atomic displacements: −0.08, +0.04, +0.03, and <0.01 Å in the first through fourth layers.

B. Adatoms and small clusters on TiN(001) and TiN(111) surfaces

Figure 1 shows low-energy surface configurations for Ti and N adatoms as well as small clusters on TiN(001). Also shown are the corresponding adsorption energy E_{ad} and cluster binding energy E_B defined as

$$E_{ad}=\frac{1}{2}\eta_N E_{N_2}+\eta_{Ti}E_{Ti}+E_s-E_{config} \quad (1)$$

Downloaded 26 May 2003 to 128.113.37.128. Redistribution subject to AIP license or copyright, see http://ojps.aip.org/japo/japcr.jsp

TABLE II. Calculated adsorption E_{ad} and binding E_B energies, as defined by Eqs. (1) and (2), on TiN(001).

TiN(001)	E_{ad} (eV)	E_B (eV)
N	−0.98	0
Ti	3.30	0
N_2	0.16	2.12
Ti_2	7.72	1.12
Ti_3	12.35	2.45
TiN	5.17	2.85
TiN_2	6.63	5.29
TiN_3	7.46	7.10
TiN_4	5.72	6.34
Ti_2N_2	13.56	8.92
Ti_2N_3	15.04	11.38
N vacancy	−2.61	—

and

$$E_B = \eta_N E_{ad,N} + \eta_{Ti} E_{ad,Ti} - E_{ad,config}. \quad (2)$$

E_{N_2} and E_{Ti} in Eq. (1) are the calculated total energies of a N_2 molecule and a Ti atom in vacuum, while η_{Ti} and η_N are the number of Ti and N adatoms considered. E_s and E_{config} are the energies of the relaxed surface and atomic configuration under investigation. $E_{ad,N}$, $E_{ad,Ti}$, and $E_{ad,config}$ in Eq. (2) are adsorption energies for single Ti and N atoms and for the cluster configuration under investigation. Binding energies defined by Eq. (2) are referenced to single adatom configurations and thus provide a measure of adatom–adatom bond strengths.

The most stable position of a single N adatom on the TiN(001) surface is shown in Fig. 1(a). The adatom bonds to a surface N with a bond length of 1.41 Å, 1.3× larger than that of a N_2 molecular bond. However, the N adatom is shifted off the on-top position by 0.83 Å along ⟨110⟩ towards a nearest-neighbor surface N. Its equilibrium position is 1.17 Å above the surface atom plane, corresponding to 55% of the bulk 001-interplanar spacing, 2.12 Å. The strongest surface atom displacement occurs for the N atom immediately below the N adatom. It shifts laterally away from the adatom by 0.15 Å along $\langle\bar{1}\bar{1}0\rangle$ and is elevated by 0.13 Å from its bulk position. This is approximately three times the relaxation displacement of a surface N atom on clean TiN(001). The N adsorption energy E_{ad}, calculated using Eq. (1), is −0.98 eV (see Table II). The negative sign signifies that N is more stable as a N_2 molecule in the gas phase than as atomic N on TiN(001). However, the adsorption energy of N referenced to atomic N in the gas phase is positive 4.16 eV. Thus, in the absence of a second N atom, atomic N strongly bonds to the TiN(001) surface. Other surface positions for the N adatom (not shown in Fig. 1) are considerably less stable. For example: E_{ad} for N above a surface Ti is −2.08 eV, directly above a surface N is −1.53 eV, and in a fourfold hollow site, similar to the Ti adatom in Fig. 1(b), is −1.56 eV.

The most stable site for Ti adatoms is the fourfold hollow shown in Fig. 1(b). The adatom primarily bonds with the two underlying N atoms which both move up 0.35 Å above their original bulk positions while the two Ti surface atoms remain essentially at their original relaxed positions. The Ti adatom is 1.70 Å above the unrelaxed position of the surface layer. This is significantly (45%) higher than the N adatom, as expected from a comparison of Ti (1.32 Å) and N (0.75 Å) covalent radii. E_{ad} for the Ti adatom is 3.30 eV in the fourfold hollow site. It decreases to E_{ad}=3.01 eV in the on-top position above a surface N and is only E_{ad}=0.57 eV above a Ti surface atom.

The lowest-energy site for a TiN admolecule on the TiN(001) surface is shown in Fig. 1(c). The Ti adatom sits on a surface N and the N adatom resides on a neighboring surface Ti atom. Since these positions are essentially those of an epitaxial overlayer, the TiN molecule can be considered as the smallest epitaxial island on TiN(001). All other configurations, including molecules along ⟨110⟩ or lower-symmetry arrangements, have higher total energies. The calculated binding energy E_B for the TiN admolecule in Fig. 1(c) is 2.85 eV. This corresponds to the energy that migrating Ti and N adatoms gain by forming TiN admdecules. E_B is 0.46 eV larger than the energy per bond of bulk TiN, 2.39 eV, obtained by dividing the calculated cohesive energy of TiN, 14.33 eV, by the number of bonds per formula unit. The strength of the Ti–N admolecule bond is also evidenced by the separation between the Ti and N adatoms, 1.75 Å, which is 18% less than the bulk TiN bond length, 2.12 Å.

N_2 molecules are only weakly physisorbed on the TiN(001) surface. A total of eight initial positions on TiN(001) were explored. In each case, the two N atoms approached each other during relaxation to a distance comparable to the gas-phase N_2 bond length, followed by an increase in separation between the N_2 molecule and the TiN surface. The calculated energies for N_2 molecules above the TiN surface are nearly independent of their exact position and orientation. Thus, no well-defined equilibrium position could be determined. Calculated total energies are all within 0.1 eV. A typical relaxed position is shown in Fig. 1(d). The N–N distance is 1.13 Å, almost identical to the N_2 gas-phase bond length, 1.11 Å. The N atoms are 2.10 and 3.18 Å above the TiN(001) surface, indicating only very weak interactions with surface atoms. This is also reflected by the fact that E_{ad}=0.16 eV is essentially negligible with respect to the computational uncertainty of ≃0.1 eV. Thus desorption of physisorbed N_2 molecules is expected to occur at near kinetic rates. E_B for the N_2 admolecule is 2.12 eV. The considerably higher stability of N_2 than single N adatoms on TiN(001) indicates that thermal dissociation of N_2 on TiN(001) is unlikely, even without considering the activation barrier for dissociation.

The most stable position of the TiN_2 admolecule is shown in Fig. 1(e) to be "L-shaped" with constituent adatoms in nearly bulk epitaxial positions. The adsorption energy E_{ad} of 6.63 eV is much larger than the value, 3.30 eV, for a single Ti adatom. Thus, a N_2 molecule can be dissociatively chemisorbed at a Ti adatom with a net energy gain of 3.33 eV. The calculated TiN_2 binding energy E_B of 5.29 eV corresponds to an energy per bond of 2.65 eV. This value is between the bond energy for bulk TiN and that for TiN-admolecules, 2.39 and 2.85 eV, respectively, following the trend noted above that the energy per bond decreases as the number of bonds increase.

Downloaded 26 May 2003 to 128.113.37.128. Redistribution subject to AIP license or copyright, see http://ojps.aip.org/japo/japcr.jsp

TABLE III. Calculated adsorption energy E_{ad} on N-terminated TiN(111).

TiN(111):N	E_{ad} (eV)
Ti	10.09
TiN	8.86
TiN_2	7.24
Ti_2	17.89
Ti_2N	18.81
Ti_2N_2	19.34
N vacancy	−0.29

Other possible admolecules containing one Ti atom, TiN_3 and TiN_4 (not shown), have adsorption energies of 7.46 and 5.72 eV, respectively. In order to investigate their stability, we calculated their energy following the loss of a N_2 molecule. Thus E_{ad} for TiN_3 is compared with that of TiN while TiN_4 is compared to TiN_2. We find that desorption of N_2 from TiN_3 results in a 2.29 eV energy decrease, while desorption from TiN_4 results in a 0.91 eV energy gain. Thus N_2 desorption is likely to occur from TiN_4 but not from TiN_3. Consequently, for film growth under high N-supply-rate conditions, TiN_2 and TiN_3 are the most stable admolecules. At lower N supply rates, Ti is expected to be present on the TiN(001) surface primarily in the form of TiN admolecules and/or atomic Ti.

During TiN film growth under low N-supply-rate conditions, Ti adatoms can form small clusters as shown in Figs. 1(f) and 1(g). The Ti adatoms occupy sites above surface N and bond primarily with the underlying TiN(001) surface, less strongly with each other, as indicated by the relatively large E_{ad} values of 7.72 and 12.35 eV with E_B of only 1.12 and 2.45 eV.

The square-shaped Ti_2N_2 island shown in Fig. 1(h) corresponds to E_{ad} and E_B values of 13.56 and 8.92 eV. The binding energy for this cluster is more than twice that of the TiN admolecule, 2.85 eV, and also much larger than E_B for TiN_2, 5.29 eV. Thus, Ti_2N_2 is more stable than both two individual TiN admolecules and a TiN_2 admolecule plus an isolated Ti adatom.

E_{ad} for a Ti adatom on a N-terminated TiN(111) surface (not shown) is 10.09 eV (see Table III), much higher than the corresponding value on TiN(001), 3.30 eV. The large adsorption energy on (111) stems from the formation of three backbonds along orthogonal ⟨100⟩ directions. TiN_i admolecules on TiN(111), including TiN and TiN_2, have lower adsorption energies, E_{ad}=8.86 and 7.24 eV, respectively, and are thus less stable than individual Ti adatoms. A pair of Ti adatoms (Ti_2) on nearest neighbor sites has an adsorption energy of 17.89 eV, less than that of two individual Ti adatoms.

The formation of N vacancies was found to be energetically unfavorable on both the TiN(001) and N-terminated TiN(111) surfaces. Calculated E_{ad} values are −2.61 and −0.29 eV, respectively.

C. Surface diffusion

Adatom surface diffusion paths were determined using a variant of the nudged elastic band method.[23] For this purpose, adatoms are moved stepwise from an initial equilibrium position to a neighboring site with the same symmetry. At each step, a structural relaxation is performed in which the adatom and the first layer [bilayer in the case of TiN(111)] atoms are relaxed. Adatom relaxation is limited to a plane perpendicular to the path between initial and final positions while surface atom relaxation is unconstrained. Figure 2 illustrates typical calculated lowest energy diffusion paths together with plots of potential energy versus position, while Table IV summarizes surface diffusion activation barriers E_s.

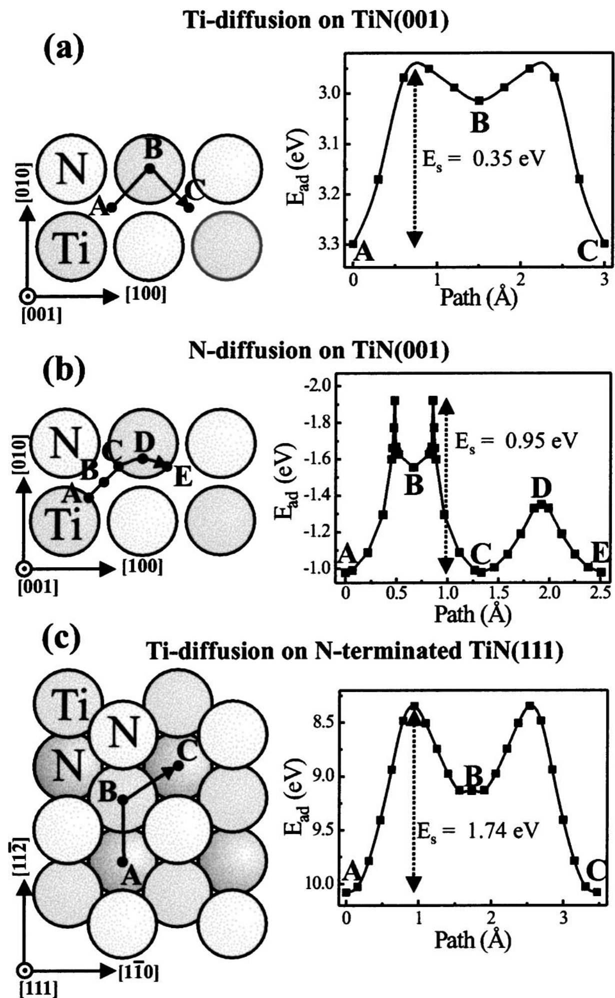

FIG. 2. Diffusion paths of (a) a Ti adatom on TiN(001), (b) a N adatom on TiN(001), and (c) a Ti adatom on N-terminated TiN(111) with corresponding plots of E_{ad} vs migration path.

The migration path of a Ti adatom along the ⟨100⟩ direction on TiN(001) is shown in Fig. 2(a). The adatom, starting from its stable fourfold-hollow site (labeled A) with an ad-

TABLE IV. Calculated surface diffusion activation energies E_s on TiN(001) and TiN(111).

Species	E_s (eV)
Ti on TiN(001)	0.35
N on TiN(001)	0.95
TiN on TiN(001)	⩾0.88
Ti on TiN(111)	1.74

Downloaded 26 May 2003 to 128.113.37.128. Redistribution subject to AIP license or copyright, see http://ojps.aip.org/japo/japcr.jsp

sorption energy of 3.30 eV, moves along ⟨110⟩ directions through a metastable site B, where $E_{ad}=3.01$ eV, above a surface N atom to the next stable site C. The two potential-energy saddle points are approximately equidistant between sites A and B, and B and C. E_{ad} is 2.95 eV at the saddle points, resulting in an activation energy E_s of 0.35 eV for Ti surface diffusion on TiN(001).

Figure 2(b) shows the migration path of a N adatom on TiN(001). Like that of Ti, it moves initially in the ⟨110⟩ direction, in this case from a stable position A ($E_{ad}=-0.98$ eV) where it is bonded to a surface N atom. The adatom moves through position B, a metastable fourfold-hollow site ($E_{ad}=-1.56$ eV), to a stable site C. The sharp peaks in the plot of E_{ad} versus distance along the pathway from A to B and B to C correspond to energy barriers of 0.95 ± 0.15 eV for breaking and forming bonds with underlying surface N atoms at a distance of 0.48 Å from the stable sites A and C. The peaks appear steep since the abscissa of the plot represents the path of the adatom, but not rearrangements of the surface atoms. For example, the underlying surface N which is initially bonded to the N adatom is displaced by up to 0.34 Å, then relaxes after bond breaking back to approximately its original position.

In addition to the above N adatom migration from A to C, the adatom also exhibits bond gyration as indicated by the path from position C to E in Fig. 2(b). Here the bond tilt rotates from $[\bar{1}\bar{1}0]$ in site C to $[1\bar{1}0]$ in site E. The energy barrier for gyration, 0.37 eV, is much smaller than the 0.95 eV required for bond breaking, indicating that the N adatom will, under typical growth conditions, rotate many times around an underlying N before it continues to a new stable site which requires breaking one N–N bond and forming a new bond with a neighboring N surface atom.

Figure 2(c) shows the diffusion path of a Ti adatom on a N-terminated TiN(111) surface. The adatom initially moves along $[11\bar{2}]$ from its stable site A to a stacking fault site B over a second layer Ti atom, and then along $[2\bar{1}\bar{1}]$ to the next stable site C. The adatom in site B ($E_{ad}=9.13$ eV) is 0.96 eV less stable than at site A ($E_{ad}=10.09$ eV). The saddle point of the diffusion path occurs at 54% of the distance between A and B with an adsorption energy of 8.35 eV, resulting in $E_s=1.74$ eV.

Diffusion of a TiN molecule on the TiN(001) surface involves a two-step process which can be visualized starting from the stable site shown in Fig. 1(c). While one adatom moves, the other remains essentially at its original position, resulting in an admolecule rotation about the surface normal. Two consecutive 90° rotations in which first one adatom of the TiN admolecule, and then the other, moves once, results in a single net admolecule migration step. Such a migration step is illustrated in Fig. 3, showing the paths of N and Ti adatoms with solid and dashed lines, respectively. We have not attempted to calculate the detailed energetics of this complex multiatom diffusion step. However, we determined energies and atomic positions of the TiN admolecule aligned along ⟨110⟩ directions, corresponding to positions B and D in Fig. 3. These configurations are exactly halfway between the stable positions A and C, and C and E, and likely represent

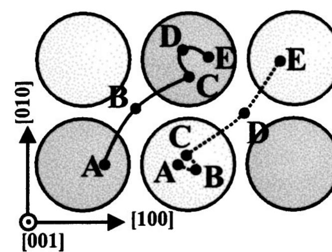

FIG. 3. The solid and dashed lines represent the paths of N and Ti atoms, respectively, during a single migration step of the TiN admolecule diffusion on TiN(001).

the saddle points. The Ti (N) adatom remains within 0.23 Å (0.19 Å) of its original position, while the N (Ti) adatom moves to a new site, as indicated by the small loop in the Ti (N) path from A to C (C to E). The adsorption energies for these ⟨110⟩ oriented TiN admolecules are 0.88 eV (0.79 eV) less than that corresponding to the relaxed position, providing a lower limit of 0.88 eV for the TiN admolecule diffusion barrier.

IV. DISCUSSION

The calculated surface energy for TiN(001), 81 meV/Å^2, is less than those for both N- and Ti-terminated TiN(111) surfaces, 85 and 346 meV/Å^2, respectively, in agreement with experimental results indicating that the (001) is the lowest energy surface.[12] Thus under film growth conditions where thermodynamics rather than kinetics control texture formation (e.g., at high growth temperatures), 001 is expected to be the dominant growth orientation.[2] However, since TiN deposition for most applications takes place at $T_s\leqslant450\,°C$ [i.e., only $\simeq0.2$ of the melting point, $T_m=2949\,°C$ (Ref. 24), in K], texture evolution will primarily be controlled by kinetics.

Comparison between surface energies of N- and Ti-terminated TiN(111) surfaces shows that the N termination is clearly favored. The difference of 261 meV/Å^2 corresponds to an energy gain of 2.03 eV/atom. Thus, bringing a Ti-terminated (111) surface into contact with N_2 gas results in an energy gain of $\simeq4$ eV per N_2 molecule in the spontaneous conversion to a N-terminated surface. This energy is considerably larger than effects due to entropy and kinetic barriers during film growth. Thus, since TiN film growth is always carried out in large partial pressures of excess N_2, we only consider fully N-terminated surfaces in this discussion.

A. TiN growth from Ti and thermal N_2 precursors

We now use the results obtained in the previous section to develop an atomic-scale understanding of the mechanisms controlling competitive 001 versus 111 texture evolution during growth of TiN films. We start by considering a layer consisting of adjacent grains with 001 and 111 orientations that are initially atomically smooth. Further, we assume a set of reasonable TiN growth conditions by magnetron sputter deposition in the fully target-poisoned regime: 10 mTorr N_2 pressure, a layer growth rate of 1 monolayer (ML) s^{-1}, and substrate temperatures of 600 and 1000 K representing typical "low" and "high" deposition temperatures, respectively.

Downloaded 26 May 2003 to 128.113.37.128. Redistribution subject to AIP license or copyright, see http://ojps.aip.org/japo/japcr.jsp

We begin by first discussing the case in which the only incident species are thermal N_2 molecules and Ti atoms. Then, we will add atomic N and energetic particles.

A pressure of 10 mTorr results in a N_2 flux of $\simeq 10^4$ ML s^{-1} incident at the growing film surface. Therefore the 111 grain is always fully N terminated. In contrast, the TiN(001) surface contains negligible steady-state nitrogen coverage, since N_2 only physisorbs on the 001 surface (E_{ad}=0.16 eV) and desorbs at near kinetic rates (10^{10}–10^{12} s^{-1}). The N_2 molecules do not dissociate on the empty 001 surface, since they are 2.12 eV more stable than single N adatoms.

Ti adatoms have relatively large adsorption energies on both surfaces, E_{ad}=3.30 eV on TiN(001) and 10.09 eV on TiN(111). Thus the Ti desorption rate from the layer is negligible at standard deposition temperatures. The incident Ti flux, which is four orders of magnitude less than the N_2 flux, therefore sets the TiN film growth rate. A Ti adatom on a 111 surface forms three strong N backbonds and, hence, has a low surface mobility. We estimate the jump rate of Ti adatoms, based upon our calculated activation energy of 1.74 eV and an attempt frequency of 10^{13} s^{-1}, to be 2×10^{-2} and 2×10^4 s^{-1} at 600 and 1000 K, respectively. The maximum mean free time t_d for diffusion of a Ti adatom (time before incorporation into the growing layer) is expected to be at least one order of magnitude less than the time required to form a ML. Thus, TiN growth at 600 K with $t_d \lesssim 10^{-1}$ s leads to essentially no Ti diffusion on 111 surfaces. Even at 1000 K, the maximum number N_d of Ti adatom diffusion steps is $\lesssim$2000. This corresponds, using a jump length $s_0 = a_0/\sqrt{2}$=3.0 Å, to a diffusion length $L = s_0\sqrt{N_d}$ of only $\simeq$130 Å.

The formation of islands is suppressed on the 111 surface since E_{ad} for two Ti adatoms on neighboring sites, 17.89 eV, is less than twice the single adatom value, 10.09 eV, indicating a Ti adatom–adatom repulsion of 2.29 eV. The repulsive interaction becomes even stronger in the presence of more Ti adatoms. E_{ad} per Ti atom for an infinite Ti island on TiN(111), obtained from the value for the Ti-terminated surface energy, is only 7.16 eV. This is almost 3 eV less than E_{ad} for the single adatom. Therefore islands do not form until the Ti surface coverage θ_{Ti} exceeds 0.33 ML, at which point the Ti adatoms are forced to occupy nearest-neighbor sites. Once this occurs, N_2 will spontaneously adsorb, within a time of 10^{-4} s, on top of the Ti cluster to maintain a stable N-terminated TiN bilayer island. In contrast, N does not adsorb on single Ti adatoms, since E_{ad} values for TiN and TiN_2 admolecules on TiN(111), 8.86 and 7.24 eV, are considerably smaller than E_{ad} for a single Ti adatom, 10.09 eV.

We define the chemical potential μ of a Ti adatom as the energy difference between a Ti atom residing in vacuum and a Ti occupying a permanent surface site. Ti adatoms reach permanent sites on the 111 surface when they form clusters. Thus, the Ti adatom chemical potential on TiN(111) is equal to E_{ad} for a single adatom, corrected by the adatom–adatom repulsion, which increases with cluster size from 2.29 eV for $i=2$ to 2.93 eV for $i\rightarrow\infty$. We therefore obtain $\mu_{Ti,111}$ values on the N-terminated surface which range, depending on the Ti cluster size, from −7.80 eV for Ti_2 to −7.16 eV for an infinite Ti cluster.

In contradistinction to the N-terminated TiN(111) case, a Ti adatom on the 001 surface, with a diffusion activation energy of only 0.35 eV, exhibits significant surface mobility. We estimate adatom hopping rates of 1×10^{10} s^{-1} at 600 K and 2×10^{11} s^{-1} at 1000 K. Thus, the Ti adatom continues to migrate on the 001 surface until it reaches an adjacent 111 grain, encounters another Ti adatom or TiN cluster, or reacts with an incident N_2 molecule. We show in the following that diffusion of the Ti adatom off the 001 grain and Ti–Ti adatom interactions are both important, while the formation of TiN_2 admolecules from Ti adatoms and gas-phase N_2 is much less likely. The latter process results in an energy gain of 3.33 eV, the difference in E_{ad} between a Ti adatom and a TiN_2 admolecule. Thus, the probability of the reaction proceeding is high. However, the probability of it occurring is low and limited by the incident N_2 flux which is 10^4 ML s^{-1}. The mean free diffusion time t_d between Ti adsorption and TiN_2 formation is $\simeq 10^{-4}$ s, resulting in $L \simeq 3\times10^3$ and 1×10^4 Å at 600 and 1000 K, respectively. Thus L for this process is $\simeq$10× to 100× the experimentally observed average grain size.[1–3]

The formation of a Ti_2 admolecule from two diffusing Ti adatoms on TiN(001) results in an energy gain E_B of 1.12 eV. The reaction probability is expected to be close to unity. Thus, the reaction rate is limited by the encounter probability which is proportional to the product of the Ti hopping rate and adatom coverage θ_{Ti}, which, assuming an empty surface at $t=0$, increases linearly with time. Using the above Ti adatom hopping rates of 1×10^{10} and 2×10^{11} s^{-1}, we calculate that Ti_2 formation is likely to start occurring at times $t_c \simeq 1\times10^{-5}$ and 3×10^{-6} s at 600 and 1000 K, respectively, following the onset of deposition. These t_c values are one to two orders of magnitude smaller than the time required for reaction of Ti with N_2 from the gas, $\simeq 10^{-4}$ s as discussed above, indicating that Ti–Ti adatom interactions occur, on average, well before nitridation of the constituent Ti adatoms. A Ti_2 admolecule is likely to grow into a larger cluster through the accretion of additional Ti adatoms. For example, the addition of a third Ti adatom to a Ti_2 admolecule yields an energy gain of 1.33 eV. Subsequent nitridation of these Ti clusters, occurring within $\simeq 10^{-4}$ s, results in the growth of TiN islands. Consequently, Ti_2 admolecules represent the primary stable nuclei for TiN(001) growth and the Ti_2 adsorption energy determines the Ti chemical potential on TiN(001). We obtain $\mu_{Ti,001} = -4.42$ eV from the calculated energy difference $(E_{ad,Ti_2} - E_{ad,Ti})$.

We calculate the Ti adatom diffusion length L on TiN(001) during the time t_c to be 1×10^3 and 2×10^3 Å at 600 and 1000 K. This corresponds to the resulting average inter-island separation which is much larger than reported average widths of columnar TiN grains, 50–200 Å.[1–3] Thus, under typical conditions for polycrystalline TiN growth, a majority of Ti adatoms will, during their diffusion on 001 grains, reach the grain boundary. We expect that a significant fraction of these adatoms will cross the boundary and, since $\mu_{Ti,111} < \mu_{Ti,001}$, remain on the adjacent 111 grain. The net lateral Ti flux from 001 to 111 grains leads, during polycrys-

Downloaded 26 May 2003 to 128.113.37.128. Redistribution subject to AIP license or copyright, see http://ojps.aip.org/japo/japcr.jsp

talline TiN deposition, to the more rapid growth of 111 grains at the expense of 001 grain growth. Therefore the width of 001 oriented grains decreases with increasing layer thickness resulting in TiN layers evolving a strong 111 preferred orientation.

The above discussion provides an atomistic explanation for experimentally observed[1–6] texture evolution towards 111, the higher surface energy orientation of TiN, under reactive magnetron sputtering conditions for which there is negligible N_2^+ ion irradiation and atomic N flux incident at the growing film. The primary reasons for texture evolution toward 111 are the large Ti adatom diffusion lengths on TiN(001) combined with the difference in Ti adatom chemical potentials for which $\mu_{Ti,111} < \mu_{Ti,001}$.

B. Role of N_2^+ ion irradiation

Magnetically unbalanced magnetron sputter deposition methods have been developed in order to investigate plasma–surface interactions during film growth.[25] In such experiments, an external magnetic field is used to shape the plasma near the substrate, resulting in an increase by up to two orders of magnitude in the ion flux incident at the growing film with essentially no effect on the sputtered atom flux. The primary advantage of this technique is that it allows independent control of ion energy, determined by the substrate bias, and ion flux. It has been applied to the growth of polycrystalline and single-crystal transition-metal nitride layers with dramatic effects on microstructural evolution and texture.[1,2,9,10,26,27] For example, TiN layers grown at 350 °C with low ion-to-Ti flux ratios, $J_{N_2^+}/J_{Ti} \leqslant 1$, and low ion energies $E_i = 20$ eV exhibit 111 texture. However, increasing $J_{N_2^+}/J_{Ti}$ to $\geqslant 5$, with all other deposition parameters remaining constant, results in 001 texture,[1,2] a total reversal.

In this section, we include the effects of low-energy, high-flux N_2^+-ion irradiation in our discussion of atomic-scale mechanisms controlling texture evolution during TiN film growth. We assume, following Refs. 1 and 2, deposition conditions which are reasonable for magnetically unbalanced magnetron sputter deposition: $J_{N_2^+}/J_{Ti} = 10$ with $E_i = 20$ eV. An ion energy of 20 eV, nearly twice the calculated N_2 dissociation energy of 10.28 eV, is sufficient for collisional dissociation of N_2^+ upon impact at the TiN surface. This provides an effective atomic N flux of $\simeq 10$ ML s^{-1} where each incident N has a calculated adsorption energy on the TiN(001) surface of -0.98 eV. The negative sign indicates that adsorbed atomic N is less stable than N_2 in the gas phase. Thus, N will spontaneously desorb from the TiN(001) surface as N_2 at rates that are limited by the N–N recombination rate. In order to estimate the steady-state atomic N coverage θ_N on TiN(001) due to N_2^+ ion impingment, we neglect possible activation barriers for N_2 recombination and desorption. From $E_s = 0.95$ eV, we calculate N hopping rates κ_N of 1×10^5 s^{-1} and 2×10^8 s^{-1} on TiN(001) at 600 and 1000 K, respectively. The bimolecular recombinative desorption rate is equal to $\kappa_N \theta_N^2$, resulting in $\theta_N = 1\times10^{-2}$ and 2×10^{-4} ML at 600 and 1000 K, respectively. These steady-state N coverages have, as discussed below, a major effect on Ti adatom diffusion and surface island nucleation on TiN(001).

Diffusing Ti adatoms on TiN(001) will, upon encountering N adatoms, form TiN admolecules with a binding energy of 2.85 eV, high enough that the dissociation rate of TiN admolecules is negligible. The average time required for a Ti adatom to encounter an N adatom is 1×10^{-8} and 3×10^{-8} s, determined based upon our calculated Ti adatom hopping rates and N coverages θ_N, at 600 and 1000 K, respectively. The number of Ti diffusion steps prior to the formation of a TiN admolecule are therefore 100 and 6000, resulting in diffusion lengths of 30 at 600 K and 200 Å at 1000 K. These values are one to two orders of magnitude less than the diffusion lengths, calculated above, in the absence of atomic N. Therefore migrating Ti adatoms are likely to form TiN admolecules before reaching a neighboring grain. However, the diffusion rate of the newly formed TiN admolecules, with an activation energy of $\geqslant 0.88$ eV, is three to five orders of magnitude slower than Ti adatom diffusion rates. Consequently, the TiN admolecule will react with additional N adatoms to form TiN_i ($i \geqslant 2$) admolecules. TiN_i admolecule binding energies increase with $i \leqslant 3$. That is, $E_B = 2.85$, 5.29, and 7.10 eV for $i = 1$, 2, and 3, respectively. However, E_B decreases for $i > 3$ (e.g., $E_B = 6.34$ for TiN_4), indicating that TiN_3 is the largest and most stable TiN_i admolecule that forms spontaneously on the TiN(001) surface. As the TiN_i admolecule number density increases, their encounter probability with other TiN_i or Ti adatoms becomes more likely, resulting in the nucleation of surface islands which continue to grow by the accretion of additional TiN_i admolecules and Ti adatoms. The growing TiN(001) islands contain approximately equal numbers of Ti and N atoms, with additional N adatoms likely terminating the edge. Further excess N desorbs as N_2 molecules.

It is clear from the above discussion that even relatively small steady-state N coverages on TiN(001) result in a dramatic reduction of the Ti adatom diffusion length. In addition, while Ti_2 admolecules are the stable nuclei for film growth on TiN(001) in the absence of atomic N, TiN_i admolecules are the critical nuclei in the presence of atomic surface N. Therefore in the presence of atomic N on the 001 surface, Ti adatoms reach their permanent sites when they join a TiN_i admolecule or a surface island. The chemical potential is estimated for the former case from the difference in E_{ad} for TiN_3 and Ti_2N_3 and for the latter by calculating E_{ad} for an infinite surface island, 9.19 eV per TiN molecule, and subtracting E_{ad} for the N adatom, -0.98 eV. Thus we obtain $-10.17\ \text{eV} \leqslant \mu_{Ti,001} \leqslant -7.58$ eV for TiN(001) growth under high flux N_2^+-ion irradiation. This is $\simeq 3$–6 eV lower than the value we obtained in the absence of atomic N on the 001 surface, $\mu_{Ti,001} = -4.42$ eV, indicative of the large effect of N_2^+-ion irradiation on TiN(001) growth kinetics. In contrast, we expect that the Ti adatom chemical potential on the 111 surface will not be significantly affected by N_2^+ ion irradiation since N does not chemisorb on N-terminated TiN(111) and desorbs from weakly bonded physisorption states at near kinetic rates. Thus, $\mu_{Ti,111}$ ranges from -7.80 to -7.16 eV while $\mu_{Ti,001} = -10.17$ to -7.58 eV for growth under high flux N_2^+-ion irradiation. While the ranges of the (111) and

Downloaded 26 May 2003 to 128.113.37.128. Redistribution subject to AIP license or copyright, see http://ojps.aip.org/japo/japcr.jsp

(001) surfaces overlap somewhat, the average value of $\mu_{\mathrm{Ti,001}}$ is $\simeq$1.4 eV less than that of $\mu_{\mathrm{Ti,111}}$, indicating that Ti adatoms are more stable on the 001 surface in the presence of atomic N on the surface. Consequently, there is a net atomic Ti flux from 111- to 001-oriented grains and the 001-oriented grains will win in competitive texture evolution under high N_2^+-ion irradiation conditions. Thus, N_2^+-ion irradiation results in a reversal of the net atomic intergrain flux and, hence, a corresponding reversal from 111 to 001 texture, in agreement with experimental results.

ACKNOWLEDGMENTS

This work was supported by the U.S. Department of Energy, Division of Materials Science, under Grant No. DEFG02-96ER45439 through the University of Illinois Frederick Seitz Materials Research Laboratory (MRL) and the Division of Materials Research, National Science Foundation. The authors also appreciate stimulating discussions with D. G. Cahill and the usage of the Materials Computation Center's IBM cluster at the MRL. The authors acknowledge support from the National Computational Science Alliance under Grant No. DMR010021N.

[1] J. E. Greene, J.-E. Sundgren, L. Hultman, I. Petrov, and D. B. Bergstrom, Appl. Phys. Lett. **67**, 2928 (1995).
[2] L. Hultman, J.-E. Sundgren, J. E. Greene, D. B. Bergstrom, and I. Petrov, J. Appl. Phys. **78**, 5395 (1995).
[3] J.-S. Chun, J. R. A. Carlsson, P. Desjardins, D. B. Bergstrom, I. Petrov, J. E. Greene, C. Lavoie, C. Cabral, Jr., and L. Hultman, J. Vac. Sci. Technol. A **19**, 182 (2001).
[4] U. C. Oh and J. H. Je, J. Appl. Phys. **74**, 1692 (1993).
[5] J. H. Je, D. Y. Noh, H. K. Kim, and K. S. Liang, J. Appl. Phys. **81**, 6126 (1997).
[6] J.-S. Chun, I. Petrov, and J. E. Greene, J. Appl. Phys. **86**, 3633 (1999).
[7] H. Huang, G. H. Gilmer, and T. D. de la Rubia, J. Appl. Phys. **84**, 3636 (1998).
[8] N. H. Hoang, D. R. McKenzie, W. D. McFall, and Y. Yin, J. Appl. Phys. **81**, 6126 (1997).
[9] D. Gall, I. Petrov, N. Hellgren, L. Hultman, J.-E. Sundgren, and J. E. Greene, J. Appl. Phys. **84**, 6034 (1998).
[10] C.-S. Shin, D. Gall, Y.-W. Kim, N. Hellgren, I. Petrov, and J. E. Greene (unpublished).
[11] J. Pelleg, L. Z. Zevin, and S. Lungo, Thin Solid Films **197**, 117 (1991).
[12] L. Hultman, J.-E. Sundgren, and J. E. Greene, J. Appl. Phys. **66**, 536 (1989).
[13] G. Kresse and J. Hafner, Phys. Rev. B **47**, 558 (1993); **49**, 14251 (1994); G. Kresse and J. Furthmüller, Comput. Mater. Sci. **6**, 15 (1996); Phys. Rev. B **54**, 11169 (1996).
[14] J. P. Perdew and Y. Wang, Phys. Rev. B **45**, 13244 (1992).
[15] D. Vanderbilt, Phys. Rev. B **41**, 7892 (1990); G. Kresse and J. Hafner, J. Phys.: Condens. Matter **6**, 8245 (1994).
[16] F. D. Murnaghan, Proc. Natl. Acad. Sci. U.S.A. **30**, 244 (1944).
[17] R. Ahuja, O. Eriksson, J. M. Wills, and B. Johansson, Phys. Rev. B **53**, 3072 (1996).
[18] M. Marlo and V. Milman, Phys. Rev. B **62**, 2899 (2000).
[19] W. J. Moore, *Physical Chemistry*, 4th ed. (Prentice-Hall, Englewood Cliffs, NJ, 1972), p. 695.
[20] This value includes a correction for the zero point energy, according to J. P. Perdew, K. Burke, and M. Ernzerhof, Phys. Rev. Lett. **77**, 3865 (1996).
[21] L. B. Pankratz, *Thermodynamic Properties of Carbides, Nitrides, and other Selected Substances* (Bulletin 696, U.S. Dept. of the Interior, Bureau of Mines, 1995), p. 823.
[22] H. J. Monkhorst and J. D. Pack, Phys. Rev. B **13**, 5188 (1976).
[23] G. Mills, H. Jónsson, and G. K. Schenter, Surf. Sci. **324**, 305 (1995).
[24] L. E. Toth, *Transition Metal Carbides and Nitrides* (Academic, New York, 1971), p. 5.
[25] I. Petrov, F. Adibi, J. E. Greene, W. D. Sproul, and W.-D. Münz, J. Vac. Sci. Technol. A **10**, 3283 (1992).
[26] F. Adibi, I. Petrov, J. E. Greene, L. Hultman, and J.-E. Sundgren, J. Appl. Phys. **73**, 8580 (1993).
[27] D. Gall, C.-S. Shin, T. Spila, M. Odén, M. J. H. Senna, J. E. Greene, and I. Petrov, J. Appl. Phys. **91**, 3589 (2002).

Downloaded 26 May 2003 to 128.113.37.128. Redistribution subject to AIP license or copyright, see http://ojps.aip.org/japo/japcr.jsp